Removal of Meropenem from Environmental Matrices by Electrochemical Oxidation using $Co/Bi/TiO_2$ Nanotube Electrodes

Amir Ahmadi,[†] Bernhard Vogler,[‡] Yang Deng,[§] and Tingting Wu[†*]

[†] Department of Civil and Environmental Engineering, The University of Alabama in Huntsville

[‡] Department of Chemistry, The University of Alabama in Huntsville

Huntsville, AL, 35899, USA

[§] Department of Earth and Environmental Studies, Montclair State University

Montclair, NJ, 07043, USA

* Corresponding author: Tel: +1-256-824-6423; email: Tingting.Wu@uah.edu

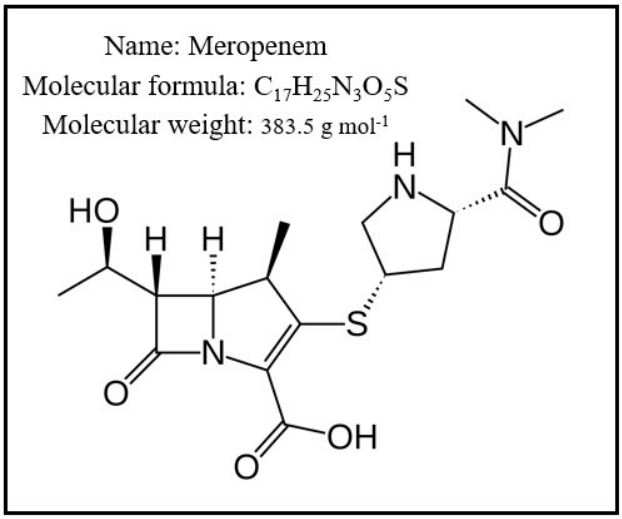

Figure S 1. Meropenem.

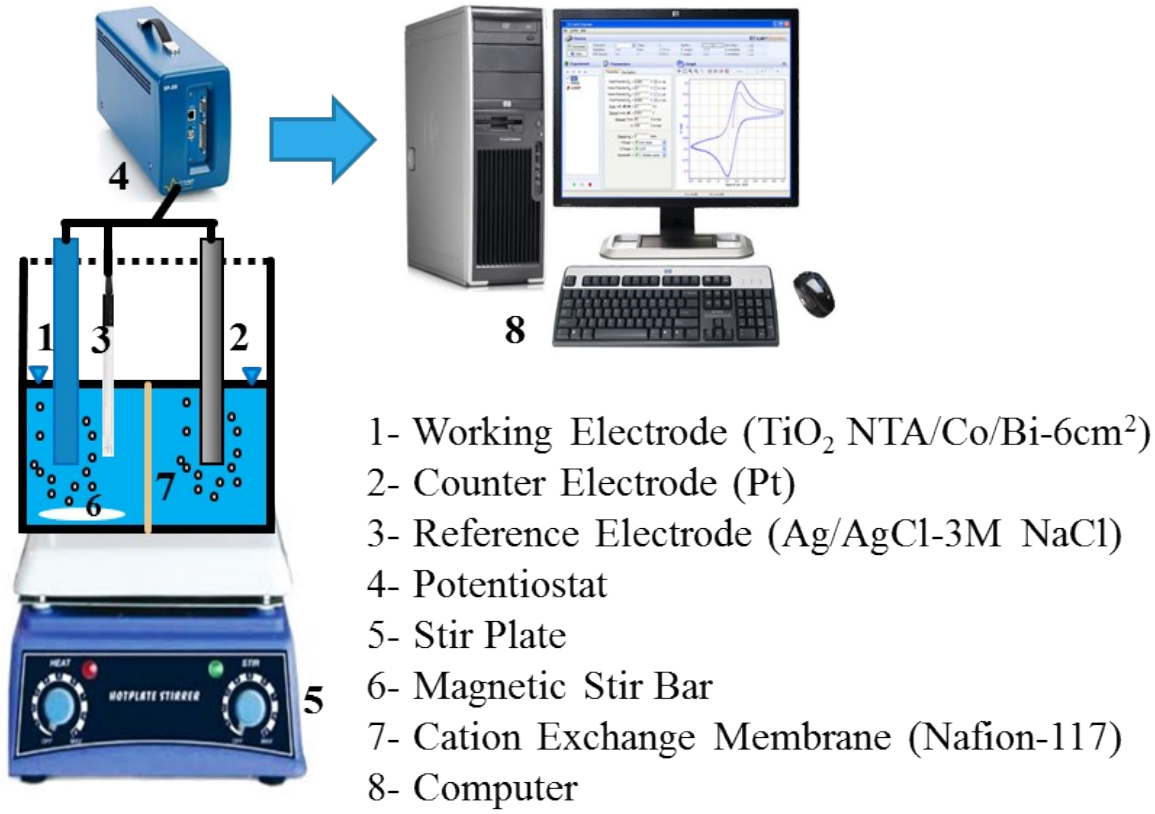

Figure S 2. Schematic diagram of the experimental setup.

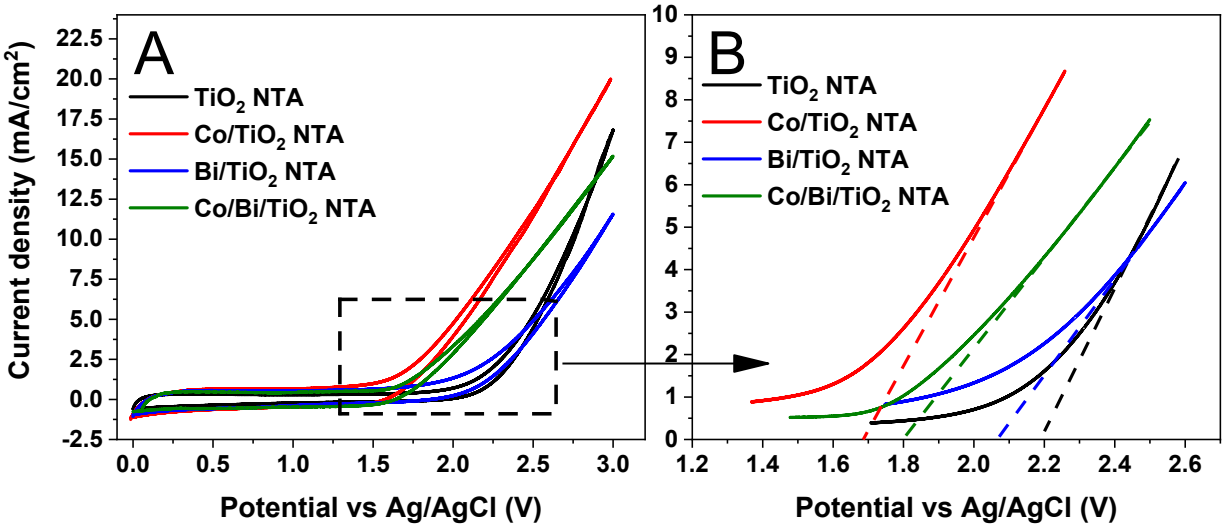

Figure S 3.Cyclic voltammetry of different TiO_2 NTA electrodes [Experimental conditions: 100 mM $NaClO_4$, Ag/AgCl (3 M NaCl) reference electrode].

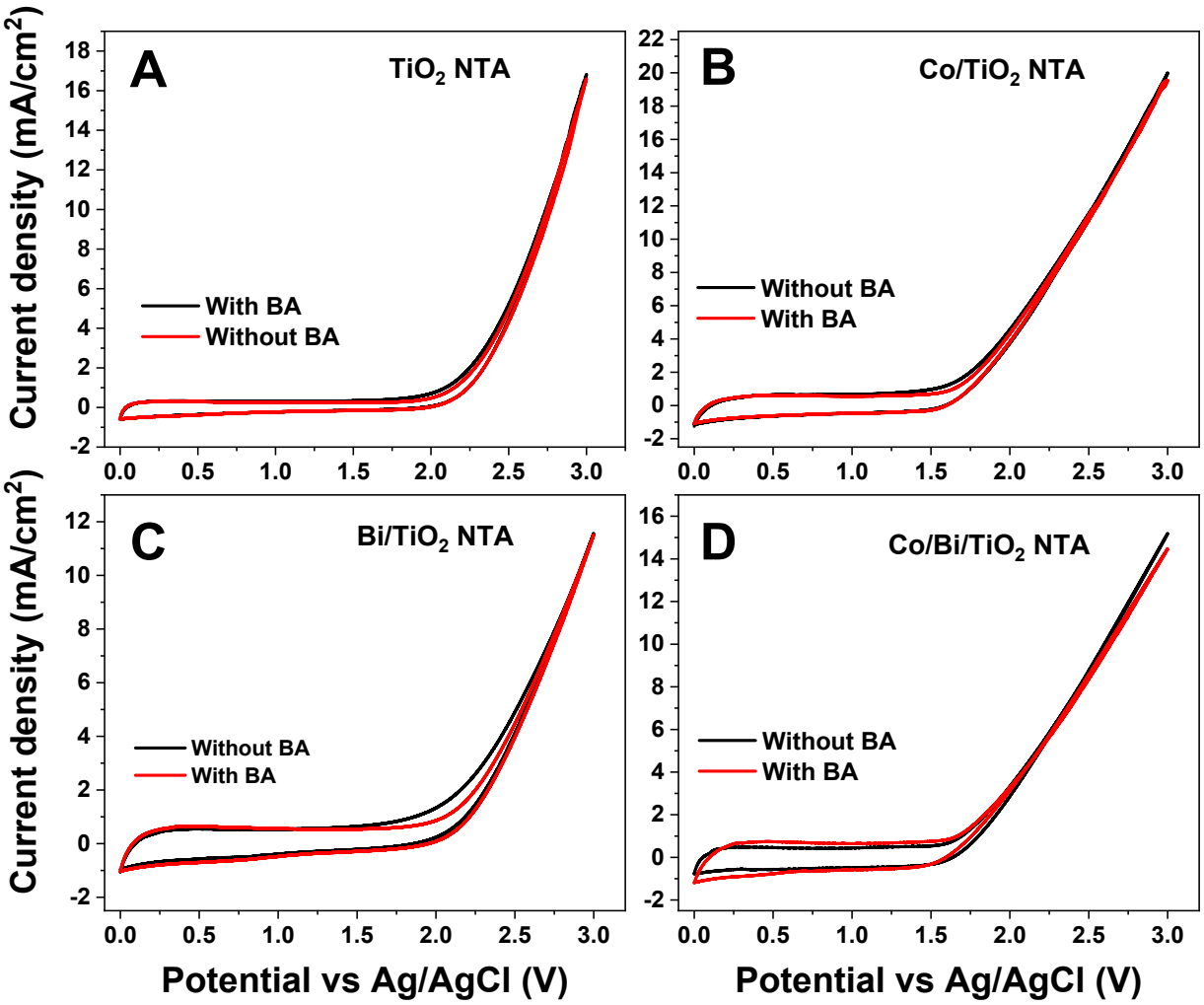

Figure S 4. Direct oxidation of BA [Experimental conditions: 1 mM BA, 100 mM $NaClO_4$, Ag/AgCl (3 M NaCl) reference electrode].

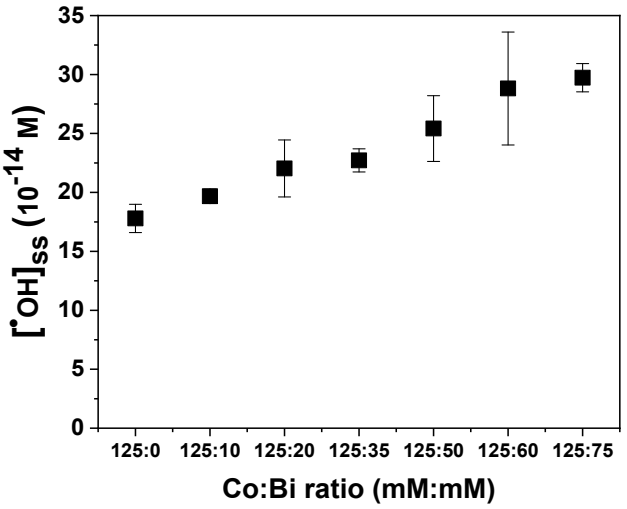

Figure S 5. $[^{\bullet}OH]_{ss}$ estimated from BA electrocatalytic degradation using Co/Bi/TiO_2 NTA electrodes with different metal doping [Experimental conditions: 1 mM BA+100 mM $NaClO_4$, Ag/AgCl (3M NaCl) reference electrode].

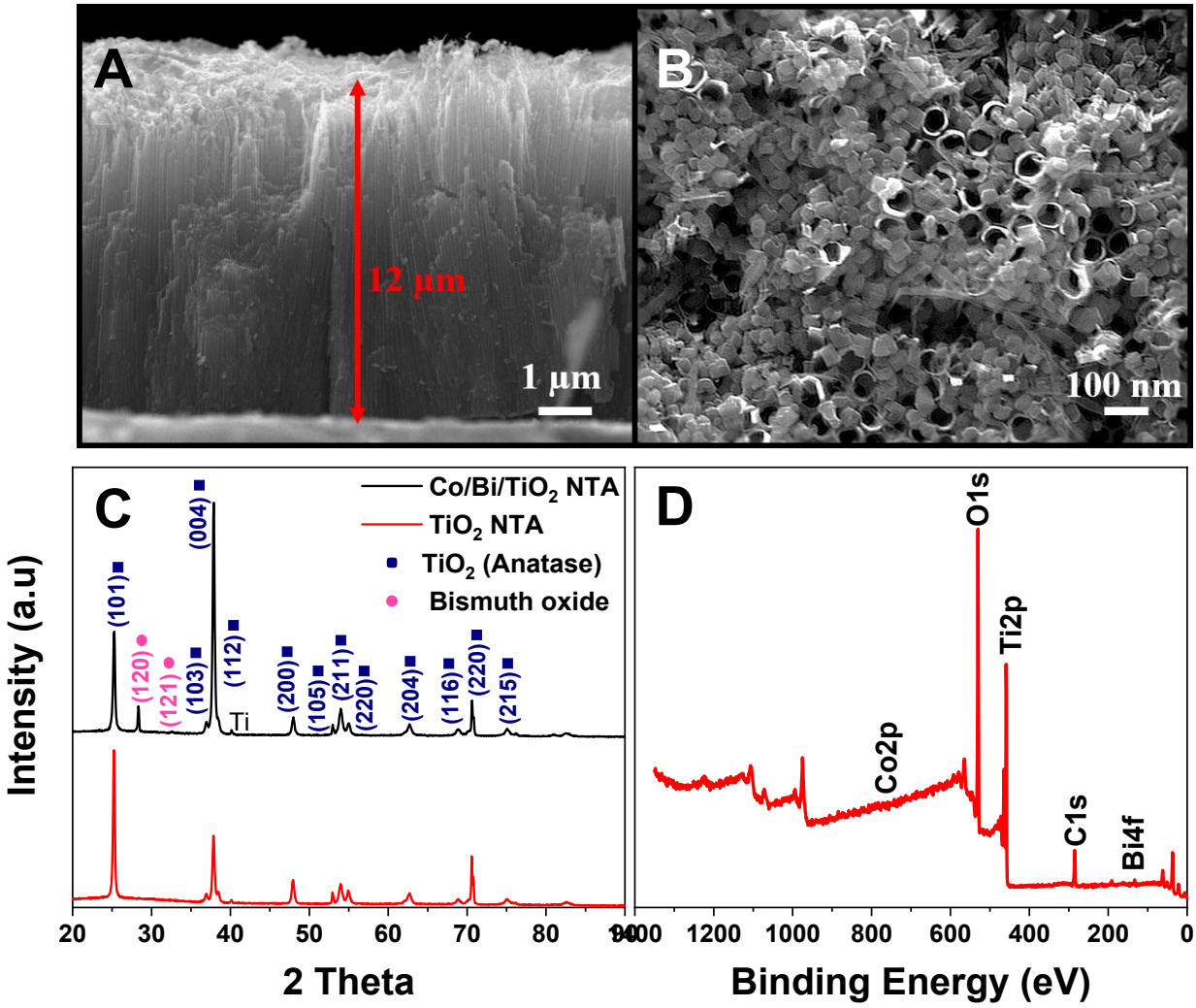

Figure S 6. A&B) SEM images; C&D) XRD and XPS spectra of Co/Bi/TiO_2 NTA electrodes, respectively.

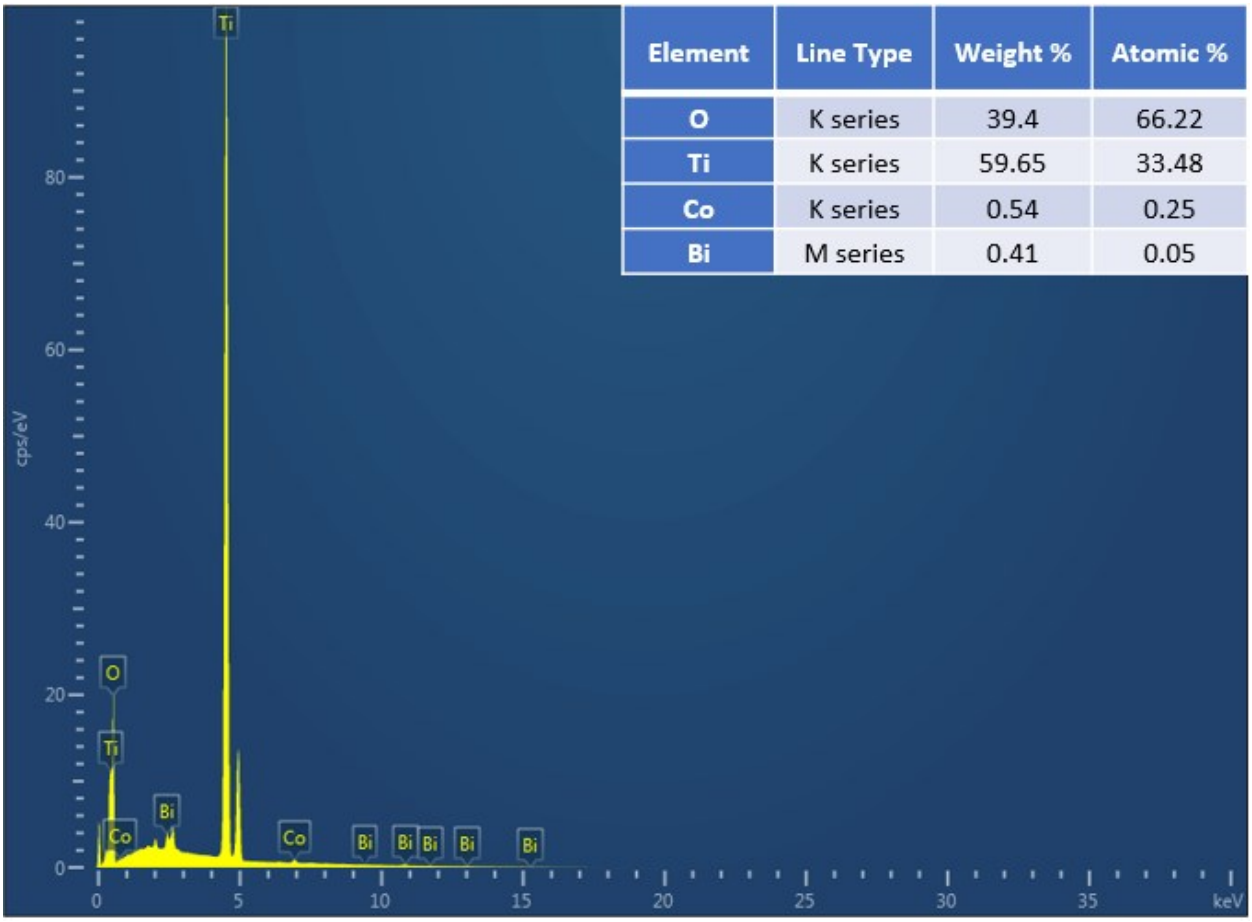

Element	Line Type	Weight %	Atomic %
O	K series	39.4	66.22
Ti	K series	59.65	33.48
Co	K series	0.54	0.25
Bi	M series	0.41	0.05

Figure S 7. EDX spectra of Co/Bi/TiO_2 NTA electrode.

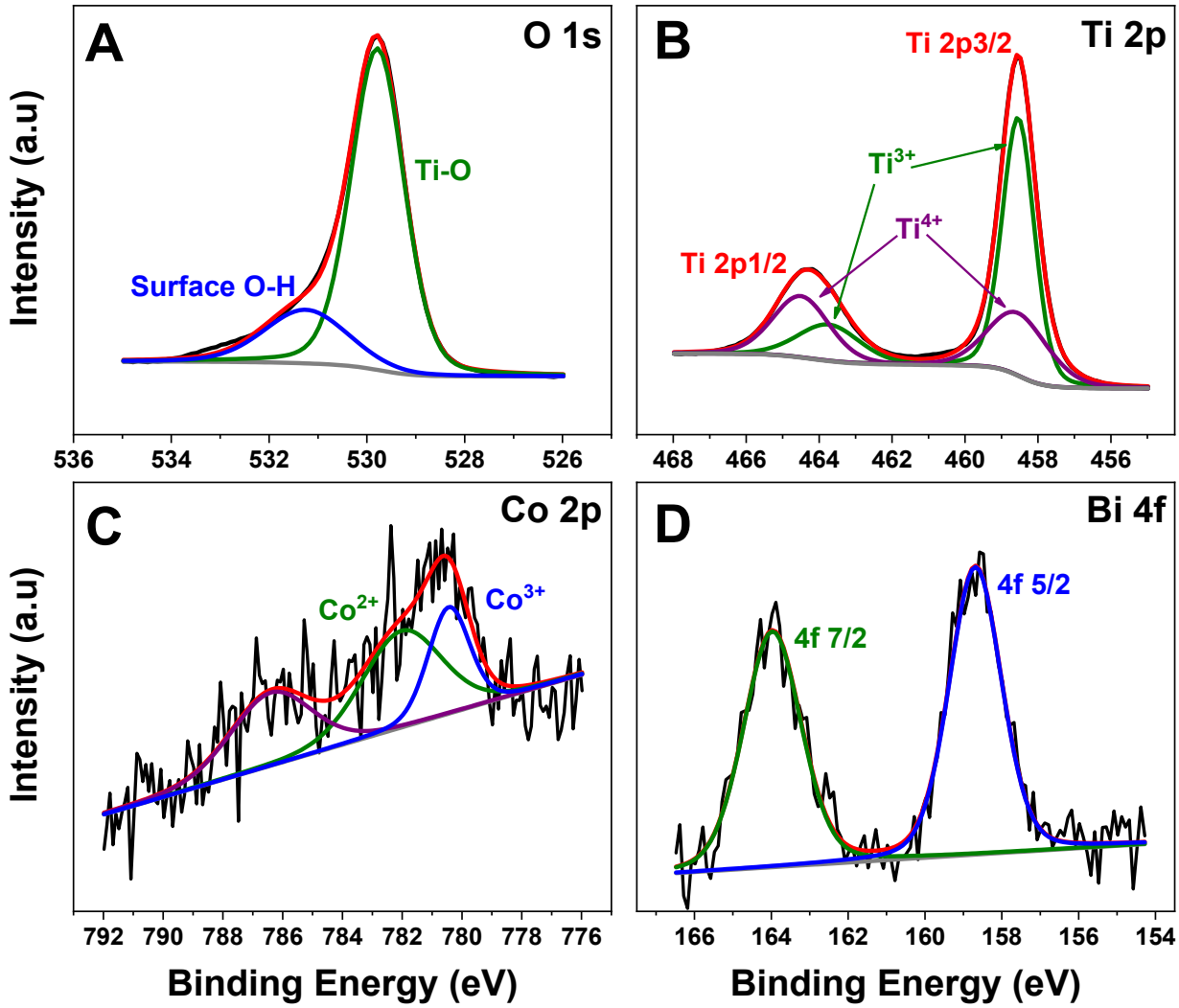

Figure S 8. XPS spectra of Co/Bi/TiO_2 NTA electrode: A) O 1s, B) Ti 2p, C) Co 2p, D) Bi 4f.

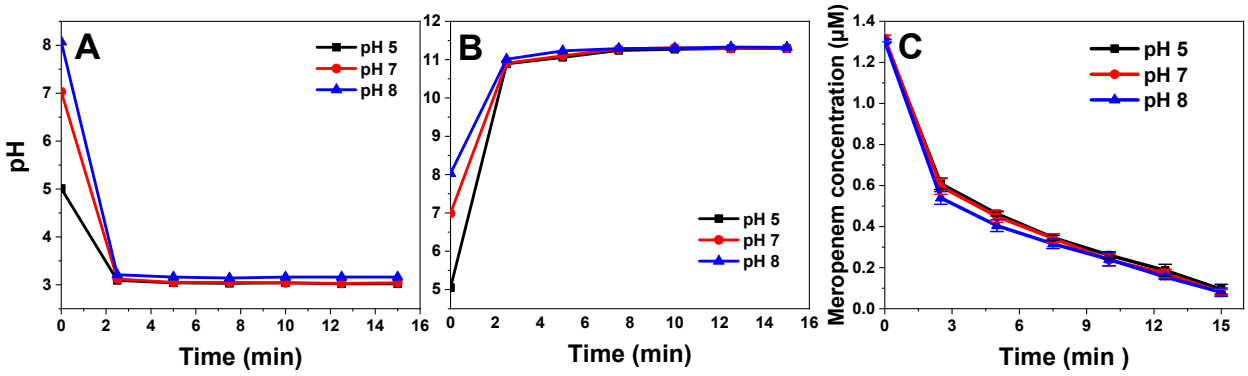

Figure S 9. pH evolution in different reactor chambers during the experiments: A) anodic chamber, B) cathodic chamber; C) Effects of initial pH on Meropenem degradation [Experimental conditions: 10 mA/cm^2, Ag/AgCl (3M NaCl) reference electrode].

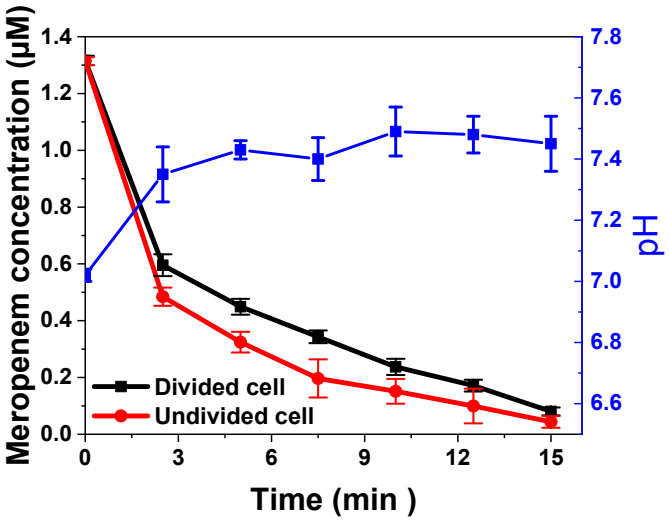

Figure S 10. Meropenme degradation in divided and undivided electrochemical cell using Co/Bi/TiO2 NTA electrode [Experimental condition: working electrode: Co/Bi/TiO2 NTA; counter electrode: Pt; applied current density: 10mA/cm^2; pH:7; background electrolyte: 30 mM $NaClO_4$; Ag/AgCl (3M NaCl) reference electrode]

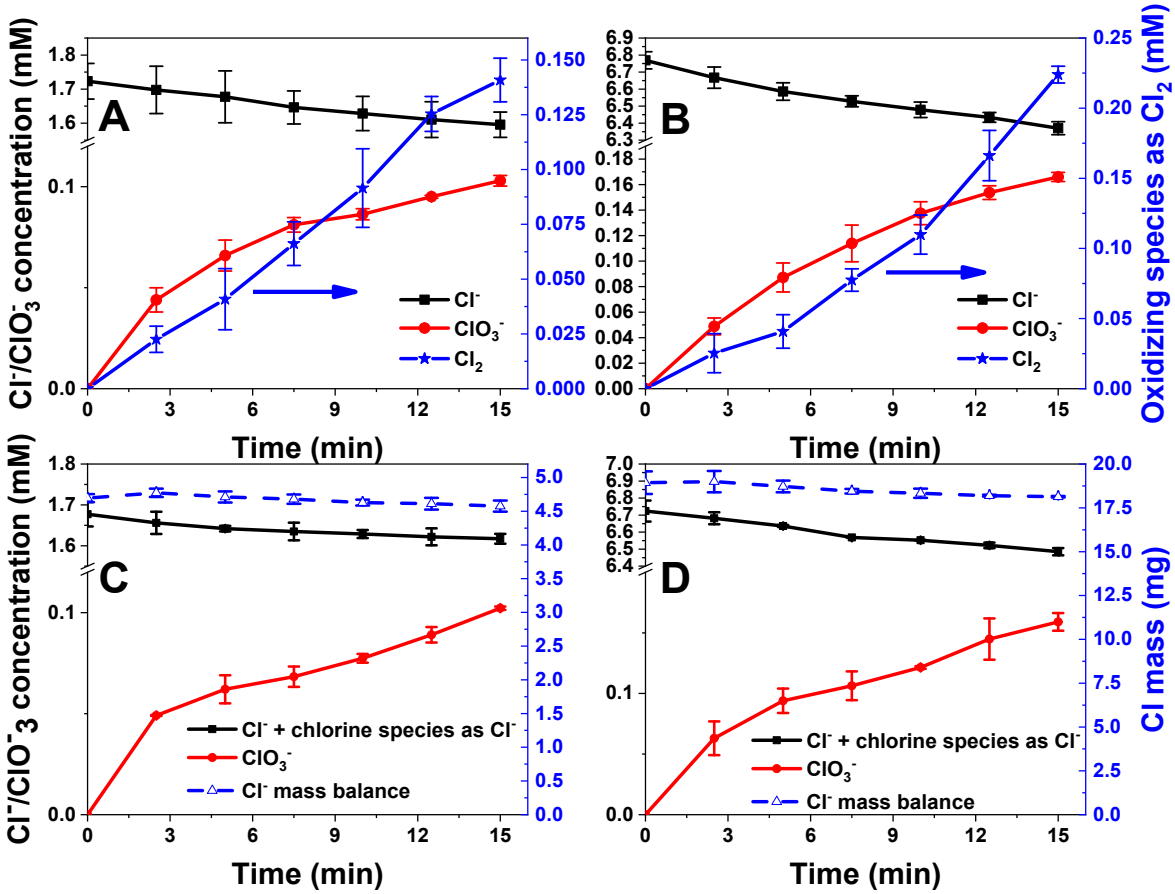

Figure S 11. Chlorinated byproduct formation and Cl mass balance: A&C) 60 mg/L Cl^-, B&D) 240 mg/L Cl^- [Experimental conditions: 10 mA/cm^2, pH 7, 30 mM Na_2SO_4, Ag/AgCl (3M NaCl) as the reference electrode in A&B, Hg/HgO (20% KOH) as the reference electrode in C&D].

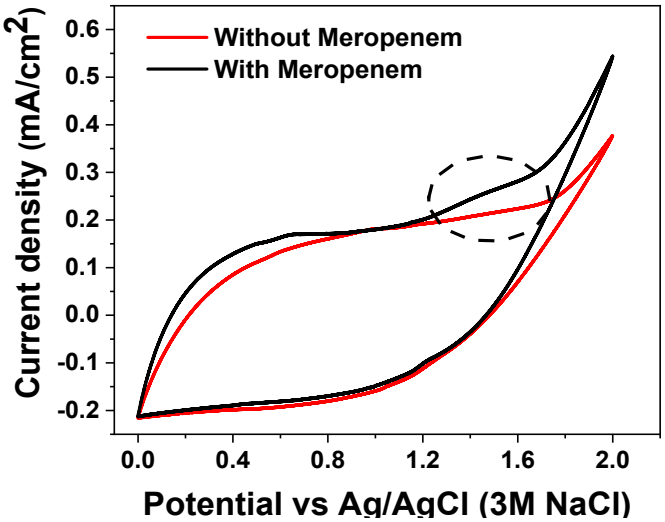

Figure S 12. Direct oxidation of Meropenem on the Co/Bi/TiO_2 NTA electrode [Experimental conditions: 5mg/L Meropenem, background electrolyte: 5 mM $NaClO_4$, sweep rate: 25mV/s, Ag/AgCl (3 M NaCl) reference electrode].

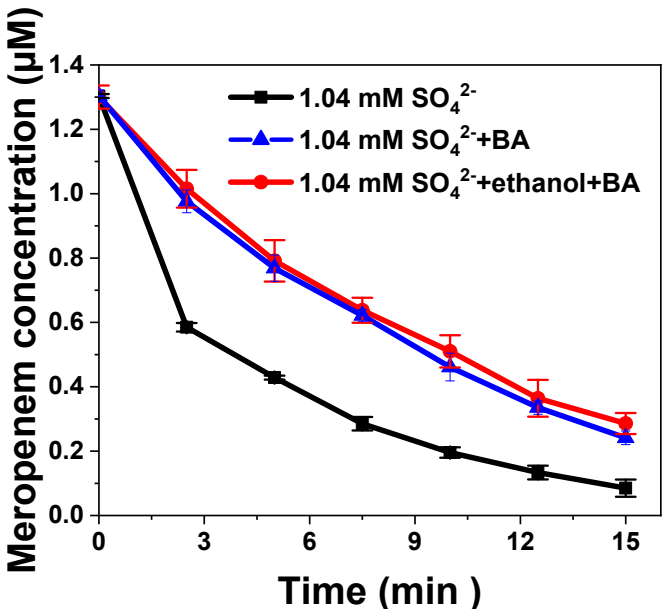

Figure S 13. Meropenem degradation in the presence and absence of scavengers [[Experimental conditions: 100 mg/L SO_4^{2-}, 100 mM ethanol, 1 mM BA, 10 mA/cm^2, pH 7, Ag/AgCl (3M NaCl) reference electrode].

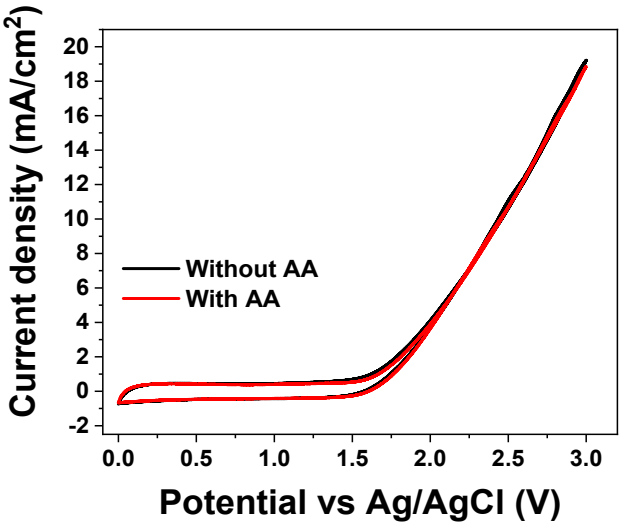

Figure S 14. Direct oxidation of AA, bicarbonate, and TBA [Experimental conditions: 100 mM $NaClO_4$ A) 100 mM AA, B) 50 mA HCO_3^-, C) 100 mM TBA Ag/AgCl (3 M NaCl) reference electrode].

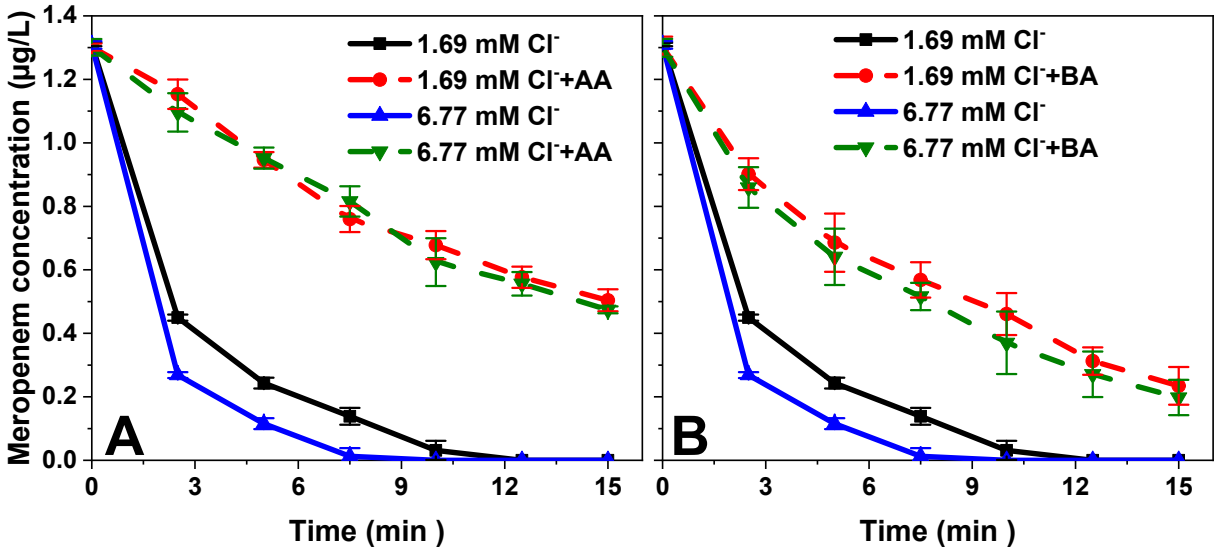

Figure S 15. Meropenem degradation in the presence and absence of RCS probe compounds [Experimental conditions: A)100 mM AA, B) 10 mM BA; Ag/AgCl (3M NaCl) reference electrode].

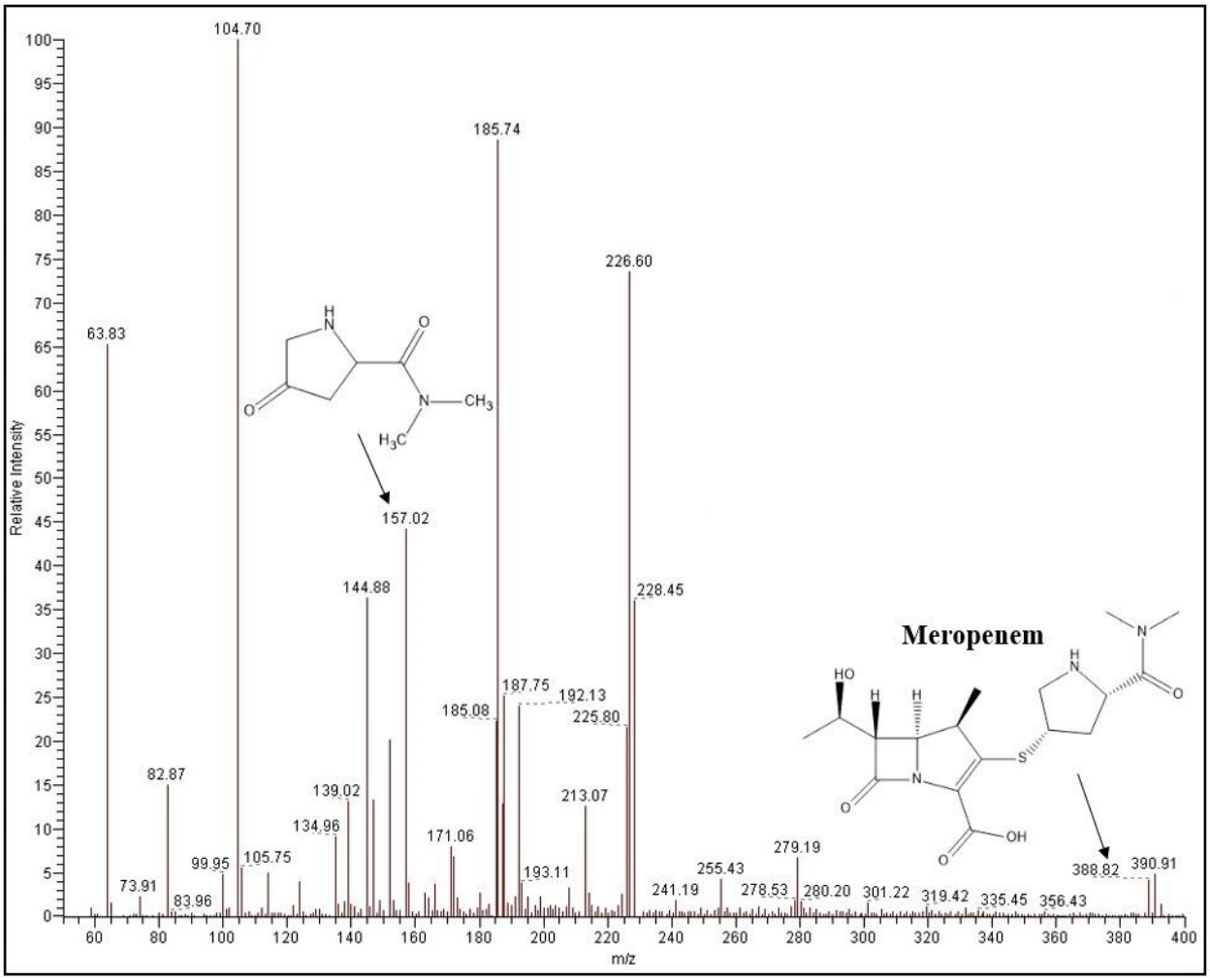

Figure S 16. LC/MS Spectrum of Meropenem transformation products in the positive EIS mode $[M+H]^+$.

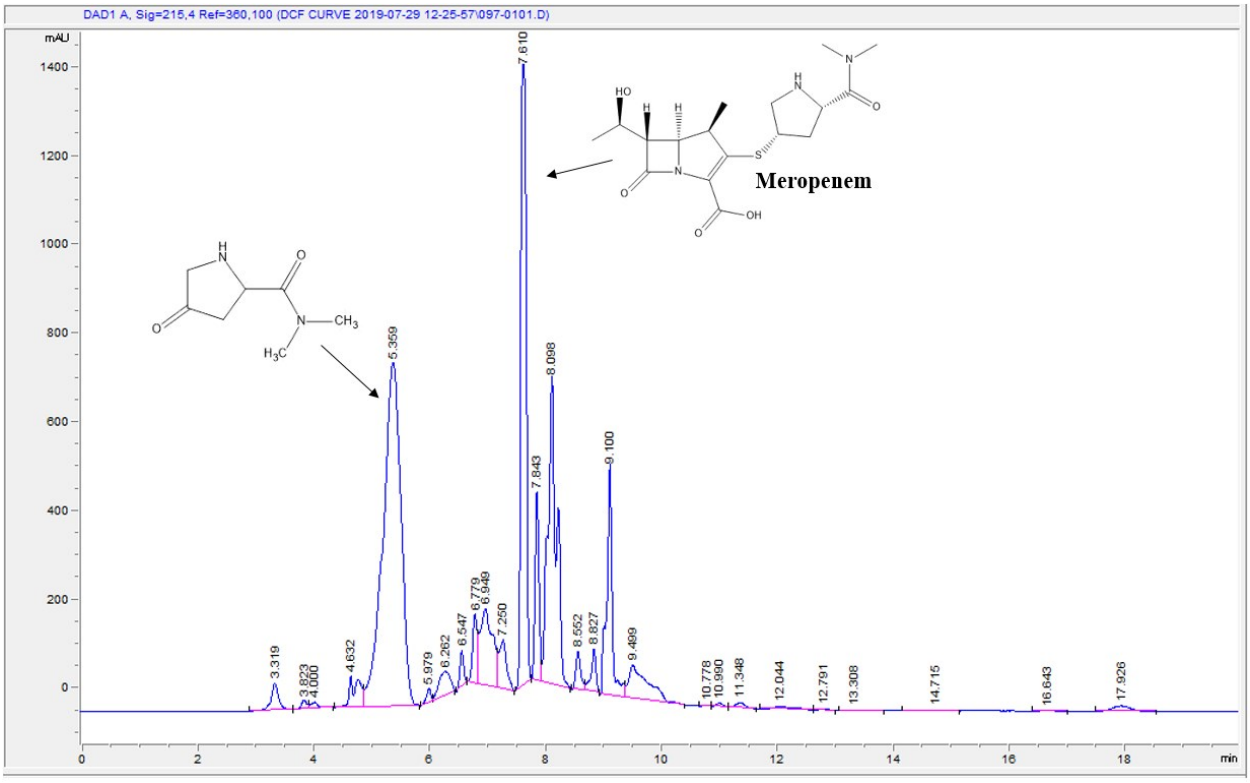

Figure S 17. HPLC/UV Spectra of Meropenem transformation products [Experimental conditions: pH=7, 10 mA/cm^2, Ag/AgCl, 15 mins electrolysis (3M NaCl) reference electrode].

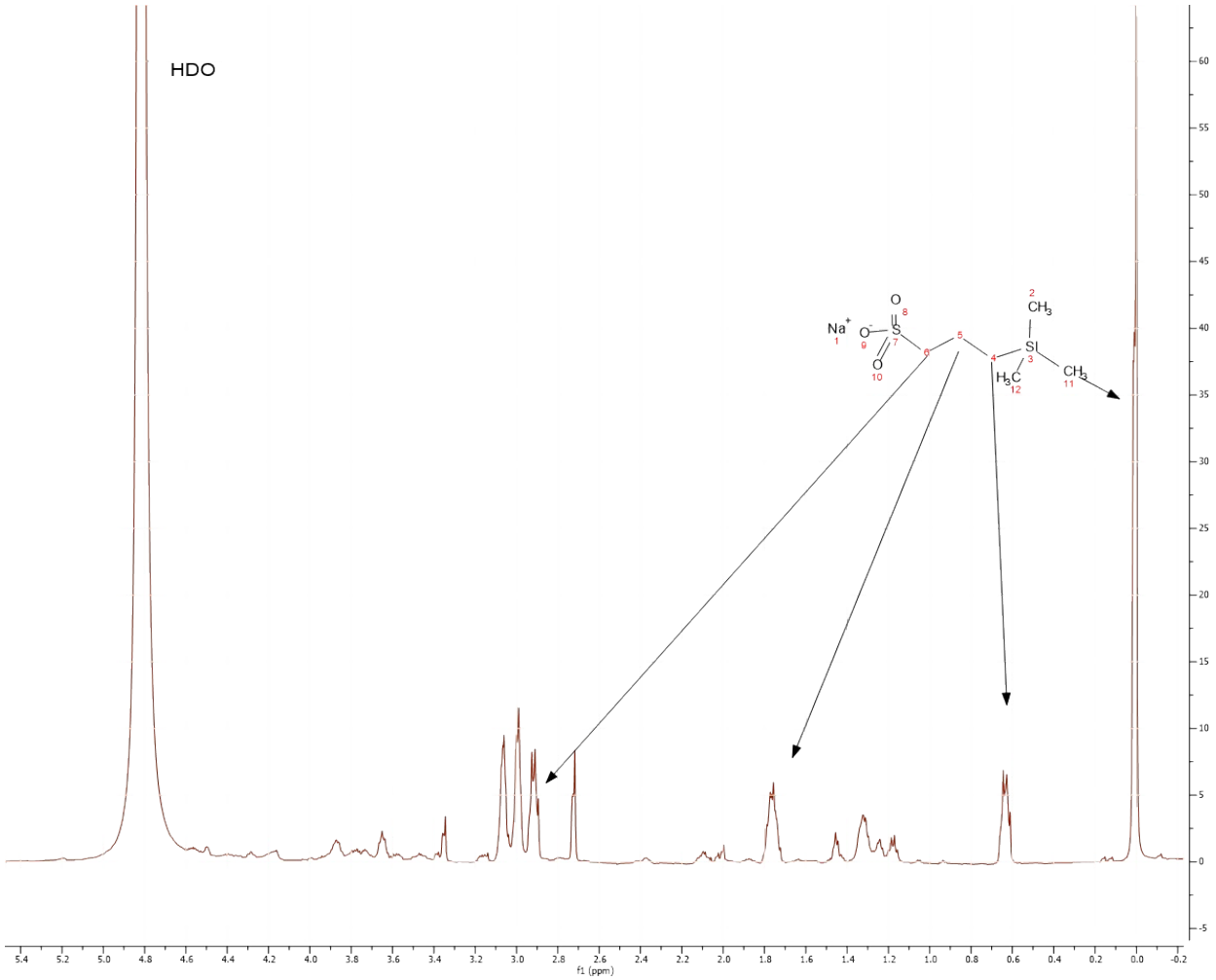

Figure S 18. ^{1}H-NMR spectrum of peak # at 500 MHz

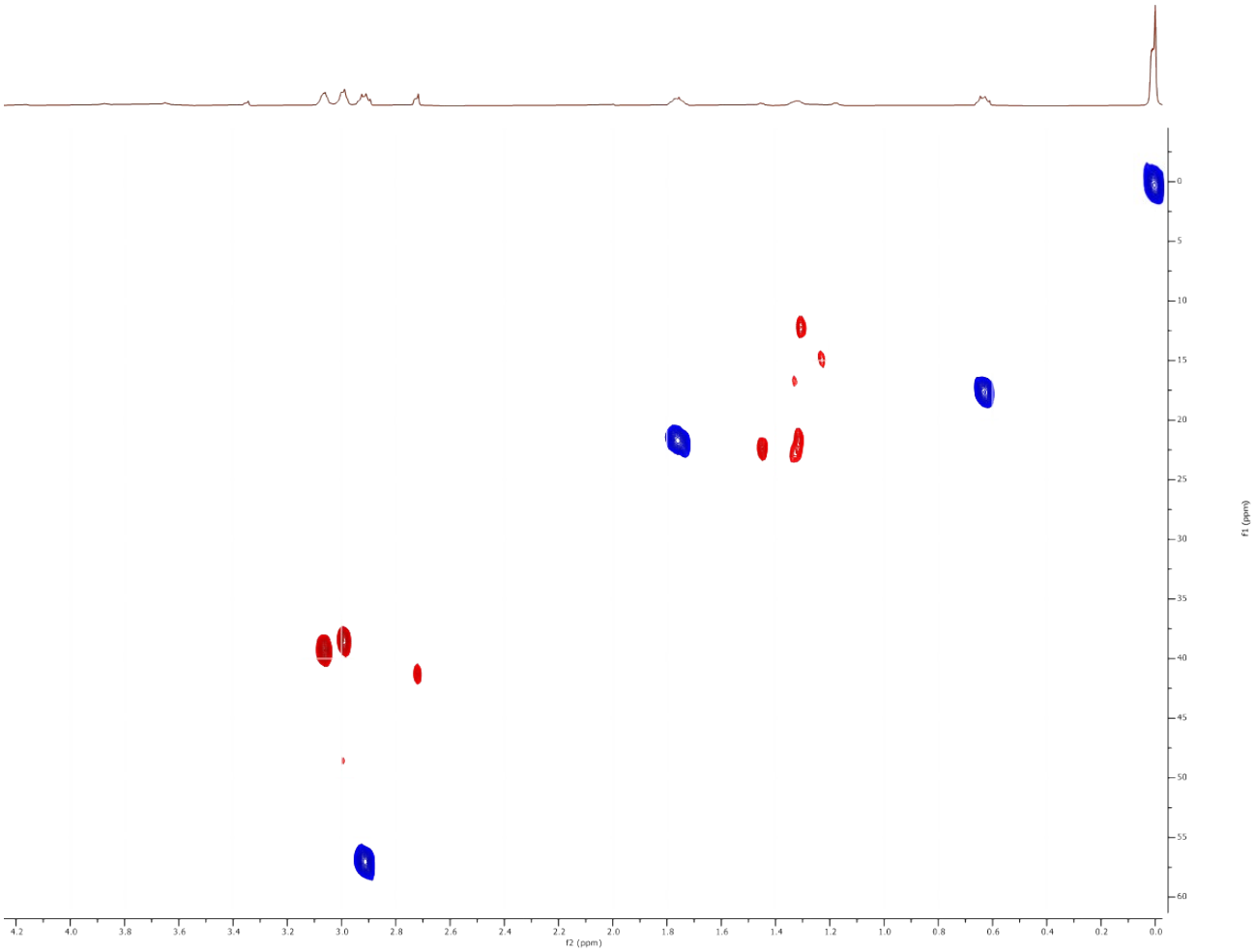

Figure S 19. HSQCSE spectrum of peak # at 500 MHz; blue peaks corresponding to DSS; red peaks due to sample.

Text S1

Meropenem trihydrate was purchased from TCI (Tokyo Chemical Industry, Japan); Benzoic acid (BA), bismuth (III) nitrate pentahydrate, and ammonium fluoride were obtained from Alfa Aesar (Massachusetts, USA); Allyl Alcohole was purchased from Sigma-Aldrich (St. Louis, USA). Other reagents were obtained from Fisher Scientific. All chemicals are of analytical grade and were used without further purification.

Text S2

Titanium foil (0.1 mm, 99.6%) was cleaned by sonication in acetone and ethanol for 10 minutes, respectively, followed by rinsing in deionized (DI) water and drying under ambient atmosphere. Then, Ti foil was anodized in an ethylene glycol (EG) electrolyte containing H_2O (2.5 wt%) and NH_4F (0.2 wt%) for 16 hours under a constant voltage of 45 V at room temperature. Subsequently, the as-formed TiO_2 NTA layer is anodized under 60 V for 5 minutes in fluoride free electrolyte (5% H_3PO_4 in EG solution) to enhance the physical stability of nanotube layer. A platinum mesh was used as the cathode in the anodization processes. After anodization, the electrode was washed with ethanol to remove remnants from the surface, and then dried naturally at room temperature.

Text S3

As shown in eqs. 1-2, the quasi steady-state concentration of $^{\bullet}OH$ ($[^{\bullet}OH]_{ss}$) during the electrolysis was estimated based on the pseudo first order rate constant of benzoic acid (BA) decay (K_{BA}) in background electrolyte (30 mM $NaClO_4$) [1]. The electrochemical behavior of BA on the surface of TiO_2 NTA-based electrodes was investigated using CV measurements (Figure S3).

130 $$\frac{d[BA]}{dt} = k_{BA,OH}\,[BA][\cdot OH] = k_{BA}[BA]$$

131 eq.1

132 $$[\cdot OH]_{SS} = \frac{k_{BA}}{k_{BA,OH}}$$

133 eq.2

134

135 **Text S4**

136 The concentration of Meropenem was measured using a high performance liquid
137 chromatography (HPLC-Agilent 1100 series) with a diode array detector (DAD) at 290 nm with a
138 Hypersil Gold 100 x 2.1 mm C18 column. The mobile phase was acetonitrile/KH_2PO_4 (20:80,
139 vol:vol%) with a flow rate of 0.2 mL/min. The benzoic acid concentration was determined using
140 the same HPLC column at a wavelength of 210 nm with a mobile phase of 30:70, vol:vol;% of
141 methano:water. Concentrations of ions (Cl^-, SO_4^{2-}, ClO^{3-}, NO_3^-, PO_4^{3-} and ClO^{4-}) were measured
142 by an ion chromatography (Thermo Dionex ICS-1600 upgraded with the RFIC system) using an
143 IonPac AS 19 anion-exchange column (4 x 250 mm), where the gradient elution was: 0→5 min
144 (10 mM KOH), 5→10 min (10→18 mM KOH) and the flow rate was 1.0 ml/min.

145

146 **Text S5**

147 The peak at 530.06 eV is attributed to the O 1s, which is fitted with two peaks at 529.78 (Ti-
148 O) and 531.28 eV(surface O-H) [2]. The Ti 2p spectra shows two peaks at 464.48 and 458.54 eV,
149 which correspond to the Ti $2p_{1/2}$ and Ti $2p_{3/2}$, respectively. These two peaks can be deconvoluted
150 into two sets of peaks. One refers to the Ti^{3+}, which is located at 458.58 and 463.76 eV, and the
151 other applies to the Ti^{4+} with binding energy at 464.58 and 458.68 eV [2]. The Co 2p pattern shows

152 two peaks at 786.28 and 780.58 eV, which were deconvoluted into three peaks centered at 786.18,
153 781.88, and 780.48 eV. The peaks located at 781.88 and 780.48 eV are attributed to Co^{2+} and Co^{3+},
154 respectively [3]. The peaks at the binding energy of 163.98 and 158.68 eV are assigned to the Bi
155 $4f_{7/2}$ and Bi $4f_{5/2}$, respectively [4].

156

157 **Text S6**

158 Effects of initial pH on Meropenem degradation and the pH evolution during the electrolysis
159 in different reactor chambers are shown in Figure S8C, respectively. While a slightly better
160 Meropenem removal was observed at pH 8 in the first 5 minutes than pH 7 or 5, overall initial pH
161 exhibited minimum effects during the treatment. Aa shown in Figure S8A, pH in the anodic
162 chamber dropped to ~3 within 2~3 min regardless of the initial value. High pH at the beginning of
163 experiment may facilitate OH^- adsorption on the electrode surface and assist the oxidation of
164 Meropenem via boosting $^{\bullet}OH$ generation[28,42].

165

166 **Text S7**

167 Chloride mass balance in synthetic electrolyte and environmental matrices:

168 Synthetic electrolyte:

169 The Cl mass balance was conducted in the synthetic electrolyte to investigate the formation of
170 chlorinated intermediate products from electrochemical oxidation of Meropenem. Here, 1.5 mM
171 $Na_2S_3O_2$ was added to the samples taken at different time intervals to quench the residual active
172 chlorine species, and then the samples were analyzed for chloride and chlorate (perchlorate was
173 not detected). The Cl mass was then calculated from the concentration of chloride and chlorate.

The formation of chlorinated products was evaluated based on the difference between the initial Cl mass and the sum of Cl mass from chloride and chlorate during the electrolysis.

Environmental matrices:

In order to examine the generation of organic chlorinated byproducts and chlorine volatile species, Cl mass balance was examined in SE and RO concentrate. First, chloride and chlorate concentrations were measured immediately after the electrolysis of environmental matrices. Since there is a chance for free chlorine species to decompose to chloride, the concentration of chloride was monitored during the following three days after the experiment. Here $Na_2S_3O_2$ was not used to react with free chlorine because it may also react with organic chlorinated byproducts such as organic chloramines. The difference between initial chloride (before electrolysis) and the sum of Cl mass in chlorate and chloride at the end may represent the formation of chlorinated byproducts and/or chlorine volatile species.

Text S8

Energy consumption is an important concern for practical applications of electrochemical treatment. In this study, the E_{EO} value was calculated using eq. 3 and data from the batch experiments [5].

$$E_{EO} = \frac{A \times I \times U \times t}{1000V \times log\left(\frac{C_0}{C}\right)} \quad \text{eq. 3}$$

where E_{EO} is the electric energy consumed to degrade the concentration of Meropenem by one order of magnitude in 1 m^3 wastewater (kWh/m^3), A is the surface area (cm^2), I is the applied current density (A/cm^2), U is the average overall potential (V), V is the volume of wastewater (m^3), t is the time of electrolysis (hr), and C is the concentration of Meropenem (μg/L).

Text S9

An empirical equation (eq. 4) was used to estimate the anodic lifetime of $Co/Bi/TiO_2$ NTA electrode [6,7].

$$T_1 \times i_1^n = T_2 \times i_2^n \qquad \text{eq. 4}$$

where, T is anodic lifetime of electrode at a constant current density (i) and n is a coefficient which can be calibrated with experimental data at different current densities. Here n = 2.135 was obtained based on the electrode lifetime at 120 and 200 mA/cm^2.

215

216

217

References

1. Yang Y, Hoffmann MR. Synthesis and Stabilization of Blue-Black TiO_2 Nanotube Arrays for Electrochemical Oxidant Generation and Wastewater Treatment. *Environ Sci Technol*. 2016:acs.est.6b03540. doi:10.1021/acs.est.6b03540.

2. Bharti B, Kumar S, Lee HN, Kumar R. Formation of oxygen vacancies and Ti^{3+} state in TiO_2 thin film and enhanced optical properties by air plasma treatment. *Sci Rep*. 2016;6(May):1-12. doi:10.1038/srep32355.

3. El Gaidoumi A, Loqman A, Benadallah AC, El Bali B, Kherbeche A. Co(II)-pyrophyllite as Catalyst for Phenol Oxidative Degradation: Optimization Study Using Response Surface Methodology. *Waste and Biomass Valorization*. 2019;10(4):1043-1051. doi:10.1007/s12649-017-0117-5.

4. Wan Y, Han M, Yu L, Yi G, Jia J. 3D Bi2S3 salix leaf-like nanosheet/TiO_2 nanorod branched heterostructure arrays for improving photoelectrochemical properties. *CrystEngComm*. 2016;18(9):1577-1584. doi:10.1039/c5ce02252e.

5. Bolton JR, Bircher KG, Tumas W, Tolman CA. Figures-of-merit for the technical development and application of advanced oxidation technologies for both electric- and solar-driven systems. *Pure Appl Chem*. 2001;73(4):627-637. doi:10.1351/pac200173040627.

6. Hine F, Yasuda M, Noda T, Yoshida T, Okuda J. Electrochemical Behavior of the Oxide-Coated Metal Anodes. *J Electrochem Soc*. 1979;126(9):1439-1445. doi:10.1149/1.2129303.

7. Chen X, Chen G, Yue PL. Stable Ti/IrO_x-Sb_2O_5-SnO_2 anode for O_2 evolution with low Ir content. *J Phys Chem B*. 2001;105(20):4623-4628. doi:10.1021/jp010038d.